SAPIENZA
UNIVERSITÀ DI ROMA

DEPARTMENT OF COMPUTER, CONTROL AND MANAGEMENT ENGINEERING

Discrete-Time Sliding Mode with Time Delay Estimation of a Six-Phase Induction Motor Drive

DIGITAL CONTROL SYSTEMS

Professor:
Claudia Califano

Students:
Filippo Federiconi
Valentina Montilii
Matteo Scuderi
Sofia Spinello

Academic Year 2024/2025

Contents

1 Introduction

Multiphase motor drives are gaining popularity in most high-power applications, like wind energy systems and electric vehicles. They're preferred to traditional three-phase drives because of some actual benefits such as reduced current/power per phase, lower torque ripple, and fault tolerance, with no need of additional hardware. On the downside, all these benefits come at the price of more difficult control laws. However, most control strategies for multiphase drives extend those of three-phase systems, including techniques like FOC, MPC and direct torque control. Some studies in the literature also include adaptations for post-fault operation, guaranteeing a certain level of performance even whenever the motor loses one or more phases. Nonlinear controllers are also widely used, for example Sliding Mode Control. This technique forces system trajectories to converge to a user-defined surface despite uncertainties, guaranteeing a good level of robustness. However, it is susceptible to the chattering phenomenon, which is deleterious for actuators. A recent approach in the literature involved combining SMC with time delay estimation (TDE). This method proved to be extremely effective in reducing chattering and improving robustness. For all these control strategies, a discrete-time implementation is essential for real world systems.

The paper analyzed for this project proposes a doble-loop discrete-time controller for an asymmetrical six-phase induction motor. The goal of the outer loop is to track a reference rotor speed ω_r^* and generate the current references for the inner feedback loop. The latter implements discrete-time SMC with TDE for tracking the reference currents.

The system model, controller design and some simulation results will be detailed in the subsequent sections.

2 Induction Motors

Induction motors are widely used in both industrial and civil applications. The most utilized version is indubitably the three-phase one, as it is embodies the best compromise in terms of performance, cost and difficulty to control. However, multi-phase (mostly 5, 6 and 9 phase) motors are more and more common, especially in applications where demanding performances are required. For example, Amazon incorporated into its transport fleet 100% all-electric Lion 6 trucks from Canadian manufacturer Lion Electric, which use six-phase induction motors. Such a large vehicle (weighting 11,800 kg) requires robust and efficient generation of significant torques and a simpler engine could not guarantee such performance.
This report focuses on a particular control technique for asymmetrical six-phase induction motors. In the next sections, a brief explanation of its functioning principles is presented, as well as a simplified structural overview.

2.1 Structure and Working Principle

Induction motors are made of two main components: a stator and a rotor. The rotor has a very particular structure called "squirrel cage" and, contrary to DC motors, has no voltage/current directly supplied.

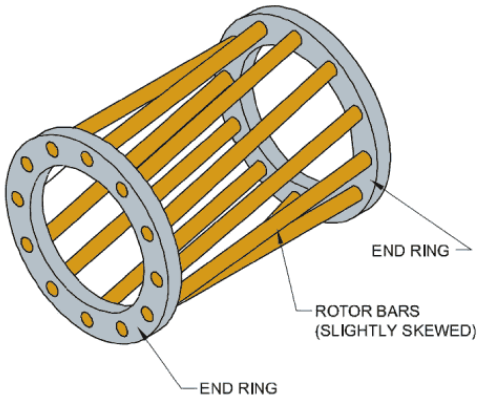

(a) Squirrel Cage Rotor

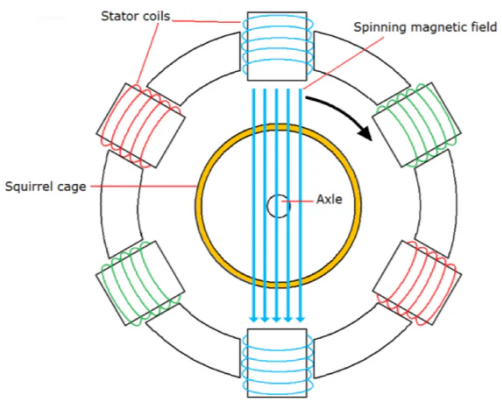

(b) Stator Windings (3-phase)

The stator instead uses some strategically placed coil windings that are supplied with AC current, to generate a rotating magnetic field.
This magnetic field interacts with the squirrel cage and induces a current on the rotor bars. The induced current also generates a magnetic field, that interacting with the stator's magnetic field makes the rotor spin. This magnetic forces' interaction produces an the rotor's mechanical torque.

The key factor for the correct functioning of the torque production is the **geometrical positioning** and **coil current** supplied to each winding (or **phase**). By positioning

the phases at a proper angle in the stator, as well as supplying them with different-phased AC currents, the resulting magnetic field rotates and creates induced current in the rotor bars. For a six-phase asymmetrical induction motor, the disposition of choice, both for the windings and for the stator currents is shown below.

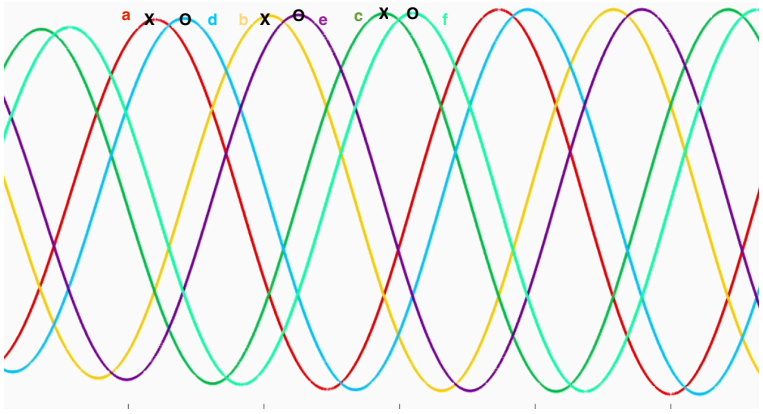

(a) Current Phase

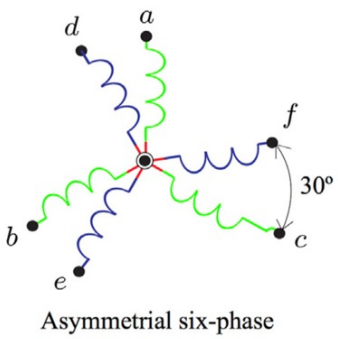

(b) Windings' Phase

The 6 phases can be divided into two groups: a-b-c and d-e-f. The elements of each group are in phase of 120° with each other, both in the current signal and in the geometric positioning of the windings in the stator. Conversely, the two groups are placed in a 30° phase with respect to each other, from which comes the adjective "asymmetric".

3 Discrete-Time Motor Model and State-Space Representation

The mathematical model of the six-phase induction motor (IM) helps to understand and manage the motor's behavior. In this section, the six-phase IM is described using a state-space model, which is based on the Vector Space Decomposition (VSD) method; this technique splits the system into separate subspaces, making it easier to design the controllers.

3.1 Six-Phase IM and VSI Model

The analyzed system consists of an asymmetrical six-phase induction motor (IM) fed by two two-level Voltage Source Inverters (2L-VSIs).

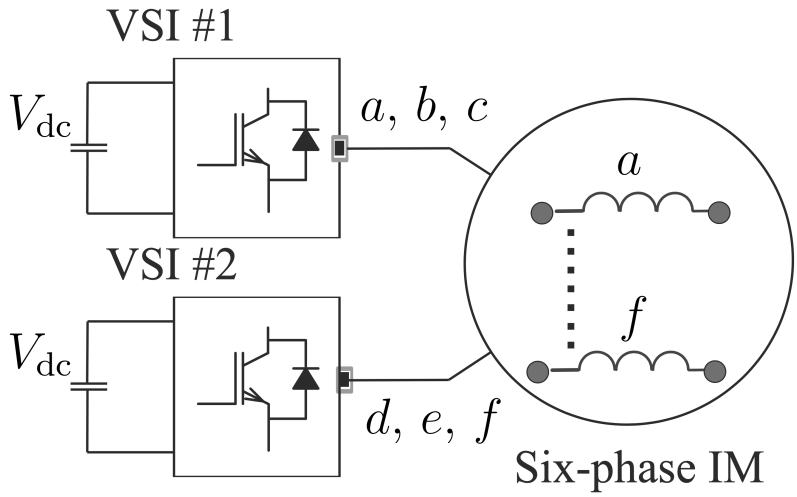

Figure 3: Scheme of the six-phase induction motor drive.

3.2 Reference Frames

The IM system has 6 inputs $[v_a, v_b, v_c, v_d, v_e, v_f]$ and most of the time only one output of interest (either torque T_e or rotor angular velocity ω_r). To control the variable of interest, it is possible to apply a **coordinate transformations** that simplify the problem using a properly defined reference frame. In this case, the vector space decomposition (VSD) method is used, in particular through the transformation matrix $\mathbf{T}$:

$$\mathbf{T} = \frac{1}{3}\begin{bmatrix} 1 & \sqrt{3}/2 & -1/2 & -\sqrt{3}/2 & -1/2 & 0 \\ 0 & 1/2 & \sqrt{3}/2 & 1/2 & -\sqrt{3}/2 & -1 \\ 1 & -\sqrt{3}/2 & -1/2 & \sqrt{3}/2 & -1/2 & 0 \\ 0 & 1/2 & -\sqrt{3}/2 & 1/2 & \sqrt{3}/2 & -1 \\ 1 & 0 & -1 & 0 & 1 & 0 \\ 0 & 1 & 0 & 1 & 0 & 1 \end{bmatrix}. \tag{1}$$

In general, the decomposition of a vector space consists in breaking down each element of the space into the sum of two vector spaces. In the case of the IM six-phase motor, applying SVD ends in having three sets of independent equation (composed by two equations) each set is referred to a precise subspace. In the end we have three subspaces:

- α-β **subspace**: Contains the flux- and torque-producing components. In this subspace live every harmonic of the form $k = 12n + 1, m = 1, 2, 3....$ This components contribute to the electromechanical energy conversion
- x-y **subspace**: Contains the loss-producing components. In this space live every harmonic of the form $k = 6n + 1, n = 1, 3, 5....$ These components are related to non-electromechanical energy conversion; in fact, there is no torque generated. In the end, this subspace is orthogonal to the $\alpha - \beta$ subspace.
- **Zero-sequence subspace**: Represents the imbalance in the currents that does not contribute to useful motor operation. In this space live every harmonic of the form $k = n - 3$

This decomposition simplifies the analysis and control of the motor by decoupling the effects of the individual stator currents into orthogonal subspaces, enabling independent control of torque, flux, and losses.

3.3 State-Space Model

The six-phase IM can be represented in state-space form after applying the VSD method. The discrete-time equations governing the system are:

$$\mathbf{x}_1(k+1) = \mathbf{A}_1\mathbf{x}_1(k) + \mathbf{H}_1\mathbf{x}_3(k) + \mathbf{B}_1\mathbf{u}_1(k) + \mathbf{n}_1(k), \tag{2}$$

$$\mathbf{x}_2(k+1) = \mathbf{A}_2\mathbf{x}_2(k) + \mathbf{B}_2\mathbf{u}_2(k) + \mathbf{n}_2(k), \tag{3}$$

$$\mathbf{x}_3(k+1) = \mathbf{A}_3\mathbf{x}_1(k) + \mathbf{H}_2\mathbf{x}_3(k) + \mathbf{B}_3\mathbf{u}_1(k) + \mathbf{n}_3(k), \tag{4}$$

$$\mathbf{y}(k) = \mathbf{C}\mathbf{x}(k) \tag{5}$$

where the state vectors are defined as:

- $\mathbf{x}_1(k) = [i_{s\alpha}(k), i_{s\beta}(k)]^\top$ (torque/flux currents),
- $\mathbf{x}_2(k) = [i_{sx}(k), i_{sy}(k)]^\top$ (loss-producing currents),
- $\mathbf{x}_3(k) = [i_{r\alpha}(k), i_{r\beta}(k)]^\top$ (rotor currents).

The input vectors are the stator voltages:

$$\mathbf{u}_1(k) = [u_{s\alpha}(k), u_{s\beta}(k)]^\top, \tag{6}$$

$$\mathbf{u}_2(k) = [u_{sx}(k), u_{sy}(k)]^\top, \tag{7}$$

The output is characterized by the stator currents:

$$\mathbf{y}(k) = [\mathbf{x}_1(k), \mathbf{x}_2(k)] = [i_{s\alpha}(k), i_{s\beta}(k), i_{sx}(k), i_{sy}(k)]^\top \tag{8}$$

and the uncertainties are represented by $\mathbf{n}_i(k)$, $i = 1, 2, 3$. The state-space matrices $\mathbf{A}_1$, $\mathbf{A}_2$, $\mathbf{A}_3$, S$\mathbf{H}_1$ and $\mathbf{H}_2$ are parameterized as:

$$\mathbf{A}_1 = \begin{bmatrix} a_{11} & a_{12} \\ a_{21} & a_{22} \end{bmatrix}, \quad \mathbf{A}_2 = \begin{bmatrix} a_{33} & 0 \\ 0 & a_{44} \end{bmatrix}, \quad \mathbf{A}_3 = \begin{bmatrix} a_{51} & a_{52} \\ a_{61} & a_{62} \end{bmatrix}, \tag{9}$$

$$\mathbf{B}_1 = \begin{bmatrix} b_1 & 0 \\ 0 & b_1 \end{bmatrix}, \quad \mathbf{B}_2 = \begin{bmatrix} b_2 & 0 \\ 0 & b_2 \end{bmatrix}, \quad \mathbf{B}_3 = \begin{bmatrix} b_3 & 0 \\ 0 & b_3 \end{bmatrix}, \tag{10}$$

$$\mathbf{H}_1 = \begin{bmatrix} h_{11} & h_{12} \\ h_{21} & h_{22} \end{bmatrix}, \quad \mathbf{H}_2 = \begin{bmatrix} h_{31} & h_{32} \\ h_{41} & h_{42} \end{bmatrix}, \tag{11}$$

where:

- $a_{11} = a_{22} = 1 - T_s c_2 R_s, \quad a_{12} = -a_{21} = T_s c_4 L_m \omega_r(k),$
- $h_{11} = h_{22} = T_s c_4 R_r, \quad h_{12} = -h_{21} = T_s c_4 L_r \omega_r(k),$
- $a_{33} = a_{44} = 1 - T_s c_3 R_s,$
- $a_{51} = a_{62} = -T_s c_4 R_s, \quad a_{52} = -a_{61} = -T_s c_5 L_m \omega_r(k),$
- $b_1 = T_s c_2, \quad b_2 = T_s c_3, \quad b_3 = -T_s c_4,$

being T_s the sampling time, R_s, R_r the stator and rotor resistances, L_s, L_r, $L_m$respectively the stator, rotor, and mutual inductances and $\omega_r(k)$ the rotor speed.
The parameters c_1, c_2, c_3, c_4, and c_5 are defined as follows: $c_1 = L_s L_r - L_m^2$, $c_2 = \frac{L_r}{c_1}$, $c_3 = \frac{1}{L_s}$, $c_4 = \frac{L_m}{c_1}$, and $c_5 = \frac{L_s}{c_1}$.
The state-space equations of the six-phase induction motor were implemented in Simulink using three distinct subsystems corresponding to the x_1, x_2, and x_3 state variables. Each subsystem computes the evolution of its respective state vector based on the discrete-time state-space representation.
The input block receives the control inputs $u(k)$, the estimated disturbances $n(k)$, and the rotor speed reference $\omega(k)$. The outputs are the updated state variables $x(k+1)$.

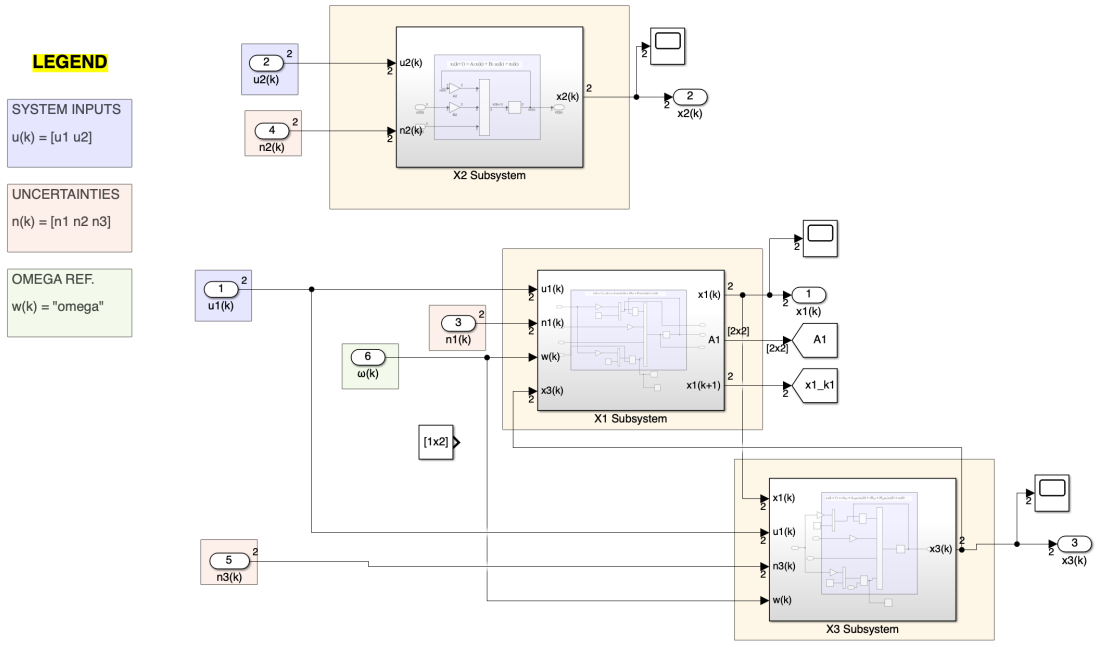

Figure 4: Simulink implementation of the six-phase induction motor state-space model. The diagram includes subsystems for the x_1, x_2, and x_3 state variables, inputs for control signals and uncertainties, and outputs for the updated state vectors.

3.4 Rotor Speed Equation

The rotor speed ω_r interacts with the electrical parameters, linking mechanical and electrical dynamics. The rotor electrical speed has in fact a relationship with load torque (T_l) and generated torque (T_e) as follows:

$$J_m\dot{\omega}_r + B_m\omega_r = P(T_e - T_l) \tag{12}$$

being B_m and J_m the friction and the inertia coefficient, respectively, P the number of pole pairs and T_e is:

$$T_e = 3PM(i_{r\beta}i_{s\alpha} - i_{r\alpha}i_{s\beta}) \tag{13}$$

where M is the magnetizing inductance.
In conclusion ω_r is computed as:

$$\dot{\omega}_r = \frac{T_e - T_l - B_m\omega_r}{J_m} \tag{14}$$

From these equations it is possible to obtain the discrete form of the rotor's angular velocity ω_r:

$$\omega_r(k+1) = \omega_r(k) + T_s\frac{P}{J_m}(T_e(k) - T_l(k)) - T_s\frac{B_m}{J_m}\omega_r(k) \tag{15}$$

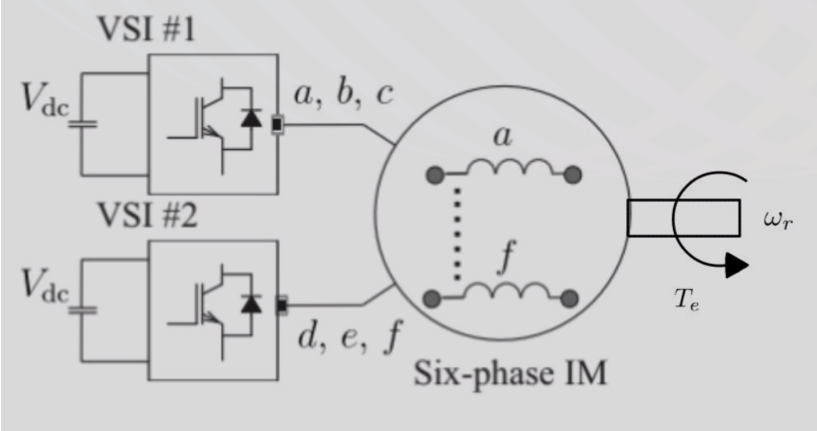

The rotor speed equation was implemented in Simulink. It models the dynamic evolution of the rotor speed, $\omega_r(k)$, based on the discretized equations of motion for the six-phase induction motor.

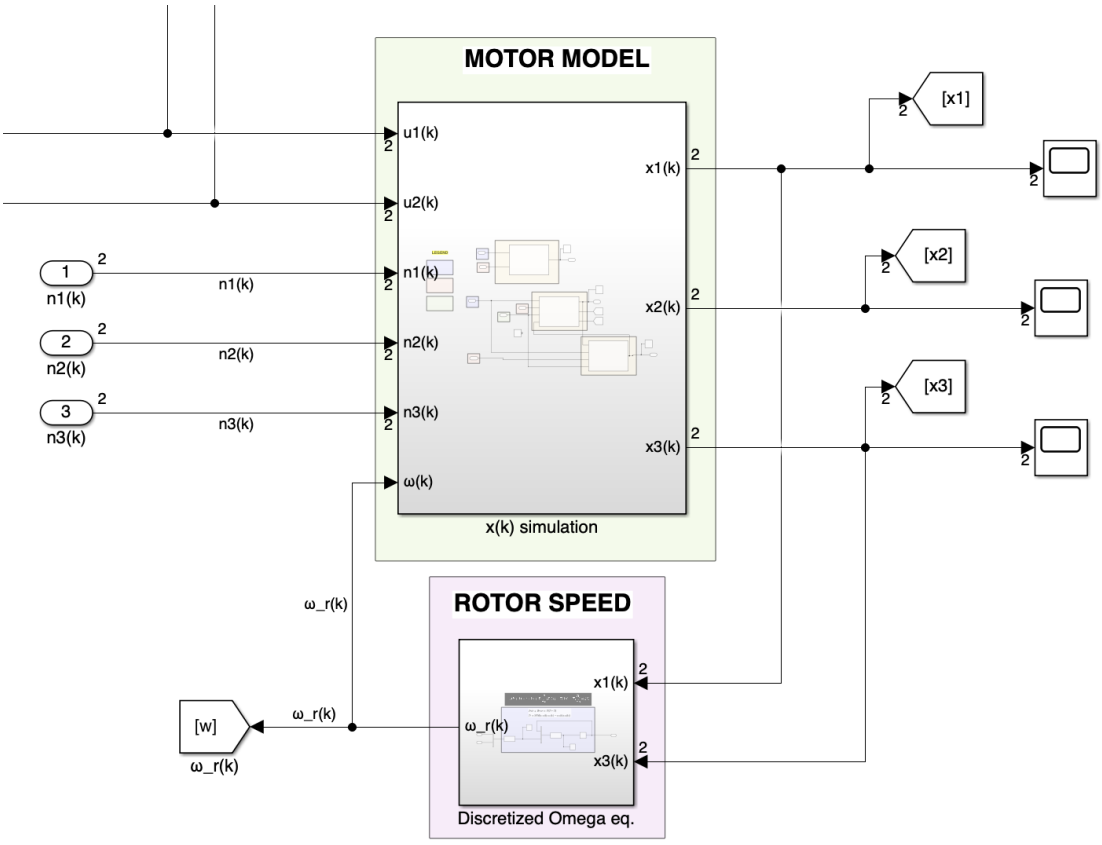

Figure 5: Motor model and rotor speed blocks.

3.5 AC Voltage Supply

As previously mentioned, contrary to DC motors, induction motors are directly supplied with current only at the stator windings. However, the voltage source is always a battery, which provides **a constant input** V_{dc}. The signal must therefore be

transformed in sinusoidal waves $[v_a, v_b, v_c, v_d, v_e, v_f]$ that serve as inputs to each phase of the IM. To do so, the considered 6-phase induction motor uses the following topology of Virtual Source Inverters (VSIs).

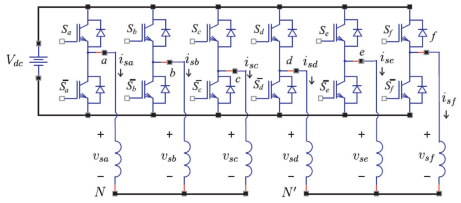

Figure 6: VSI topology for 6-Phase IM

A VSI is a type of converter that converts DC Voltage to AC Voltage. It is composed of a DC power source, transistor (MOSFET) for switching, and a DC link capacitor. An ideal VSI keeps the voltage constant throughout the process.

In the VSI model, the relationship between the stator voltages and the gating signals is given by:

$$\begin{bmatrix} u_{s\alpha}(k) \\ u_{s\beta}(k) \\ u_{sx}(k) \\ u_{sy}(k) \end{bmatrix} = V_{dc}\, \mathbf{T}\, \mathbf{M}, \tag{16}$$

where:

- V_{dc} is the DC-bus voltage,
- $\mathbf{M}$ is the modulation matrix, defined as:

$$\mathbf{M} = \frac{1}{3} \begin{bmatrix} 2 & 0 & -1 & 0 & -1 & 0 \\ 0 & 2 & 0 & -1 & 0 & -1 \\ -1 & 0 & 2 & 0 & -1 & 0 \\ 0 & -1 & 0 & 2 & 0 & -1 \\ -1 & 0 & -1 & 0 & 2 & 0 \\ 0 & -1 & 0 & -1 & 0 & 2 \end{bmatrix} \begin{bmatrix} S_a \\ S_b \\ S_c \\ S_d \\ S_e \\ S_f \end{bmatrix}, \tag{17}$$

  where $S_i \in \{0, 1\}$ are the gating signals of the inverters.

Figure 3 illustrates the block diagram of the six-phase induction motor drive. The stator windings of the motor are organized into six phases, denoted as a, b, c, d, e, and f. The currents flowing through these windings, $i_a, i_b, i_c, i_d, i_e, i_f$, are the primary variables used to control the motor. Each of these currents corresponds to a specific stator phase and contributes to generating the rotating magnetic field within the motor. To establish the relationship between the stator voltages and the inverter

signals, assume the gating signals S as ideal. In each Voltage Source Inverter (VSI), there are 8 possible gating signals, corresponding to the following combinations of the upper and lower switches for each phase:

$$(0,0,0),(0,0,1),(0,1,0),(0,1,1),(1,0,0),(1,0,1),(1,1,0),(1,1,1)$$

For each signal, the logic is as follows: - If $S_a = 1$, the upper switch of phase a is turned ON while the lower switch is OFF, and the same logic applies to the other phases. - The signal combinations $(0,0,0)$ and $(1,1,1)$ represent zero vectors, while all other combinations correspond to active vectors that drive the motor.

This gating logic is essential for the proper operation of the inverters, ensuring that the correct phase voltages are applied to the motor according to the control strategy. The parameter V_{dc} represents the DC bus voltage. It is the direct current voltage supplied to the inverters in a six-phase induction motor drive system.
In a typical Voltage Source Inverter (VSI) setup, the DC voltage V_{dc} is converted into a controlled AC voltage to supply the motor. The relationship between the DC bus voltage, the transformation matrix $\mathbf{T}$, and the modulation matrix $\mathbf{M}$ defines the stator voltages $u_a, u_b, u_c, \ldots$, as shown previously. These stator voltages are responsible for generating the rotating magnetic field within the motor, which is essential for torque production and motor operation. The value of V_{dc} directly affects the performance of the motor. A higher V_{dc} allows for higher maximum output voltages from the inverter, enabling greater control over the motor's speed and torque.

3.5.1 Clarke Transform

The Clarke (or $\alpha - \beta$ transformation), in our case in particular, can be used to reduce the dimensionality of the problem thanks to a subspace decomposition.

- $\alpha - \beta$ **subspace:** flux/torque producing components
- $zero - sequence$ **subspace:** approximately zero under normal conditions

With the hypothesis of "normal" operating conditions, the zero-sequence component can be discarded and therefore the dimensionality of the state space is reduced from 3 to 2. The control inputs can also be reduced from $[v_a, v_b, v_c]$ to $[v_\alpha, v_\beta]$ applying the linear transformation:

3.5.2 Park Transform

The Park (or Direct-Quadrature-Zero) transformation is very useful for reference tracking. It considers a rotating reference frame (with speed equal to the rotor speed ω_r).

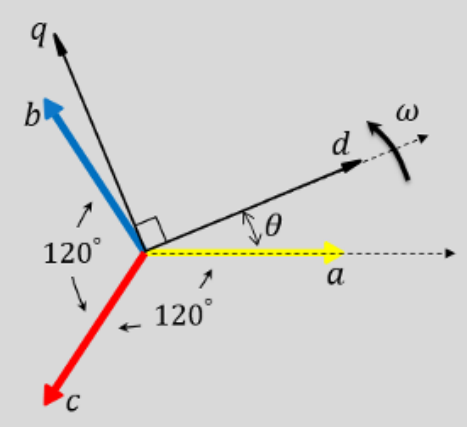

Figure 7: Visualization of the Park Rotating Reference Frame

The vector representing the total current contribution to the magnetic field can therefore be decomposed into the two directions (direct and quadrature). Since the reference frame rotates with the rotor itself, the decomposed currents i_d, i_q are **constant** (not sinusoidal). This is incredibly useful for utilizing classic controllers (such as PIDs), where dealing with constant references is much easier than sinusoidal ones.
The two frameworks (Clarke and Park) are used together in more complex control schemes (often with multiple feedback loops) to simplify the problem, depending on the specific control objective.

4 Sliding Mode Control (SMC)

4.1 Principle of Sliding Mode

Sliding mode control is a robust nonlinear control technique that forces the system's state trajectories to converge and remain on a predefined switching surface in finite-time, even in presence of disturbances. Given a general continuous-time system:

$$\dot{x} = Ax + Bu$$

determine:

- a switching function $s(x)$ such that the sliding mode on the switching plane $\sigma = \{x : s(x) = 0\}$ is stable
- a high-speed switching control law

$$u(x) = \begin{cases} +u_0 & \text{if } s(x) > 0 \\ -u_0 & \text{if } s(x) < 0 \end{cases}$$

  that stabilizes the system along the sliding surface.

This implies that the state, starting from any initial state, will move toward the switching plane and arrive in finite time.

Sliding mode systems are characterized by a finite time interval for reaching the sliding manifold $\sigma = \{x : s(x) = 0\}$, calling t_{sm} the time in which the system is in 'sliding mode':

- for t $\geq t_{sm}$ the trajectory motion is confined in the manifold $\sigma = \{x : s(x) = 0\}$
- for $t_{sm} \geq$ t it is not possible to reverse calculate the trajectory, then it cannot be backtracked beyond the manifold $\sigma = \{x : s(x) = 0\}$.

The discrete-time representation:

$$x(k+1) = Ax(k) + Bu(k)$$

starting from t_{sm}, the state trajectory belongs to the sliding manifold:

$$s(k) = 0 \quad \forall\, k \geq k_{sm}$$

The discrete-time control law, which generates the sliding mode derives from selecting $u(k)$ at each sampling point k, such that this control input will achieve $s(k+1) = 0$ at the next sampling point $(k+1)$.

Thus, the manifold is reached after a finite time interval $t_{sm} = k_{sm}\Delta t$ and thereafter the state $x(k)$ remains on the manifold.

4.2 Chattering Phenomenon

A major drawback of SMC is due to high frequency switching over discontinuity of control signal, time-delay, and unexpected disturbances, especially in implementation. To avoid this phenomenon, it is possible to use a continuous function, such as the saturation function, instead of the sign function, or to design a robust observer instead of the controller, integrate the control input so the discontinuous term acting on its first derivative becomes continuous, or to design the controller in discrete time.

4.3 Real-Time Discrete Implementation

To implement sliding mode control there exist two options:

- analogue implementation of discontinuous control law
- direct discrete implementation with digital controller and discretization chatter.

The advantage of designing the controller in discrete time is the real-time implementation, mostly executed through discrete systems, and the maintenance of the intrinsic characteristic of the sliding mode.

Plus, there's no more the problem of chattering due to high-frequency, present in continuous time systems; this is because for a discrete system a quasi-sliding mode band is determined and around it a quasi-sliding mode always exists. Such band inherently serves as a "boundary layer"; within this layer, the trajectories remain confined, which effectively suppresses the high-frequency oscillations.

The motion of a discrete time system is called a quasi-sliding mode, because it is not possible to meet in practice an ideal trajectory of the system, where the state must arrive at the switching plane exactly at the switching time, and the dynamics of the system must match the one of the ideal switching plane to enable the state to slide on the switching plane.

The key benefits of discrete-time SMC include its suitability for digital implementation and its ability to mitigate high-frequency oscillations. Nonetheless, its design must balance sampling rates with control precision. When implemented properly, discrete SMC delivers strong disturbance rejection, robustness, and efficient computation.

4.4 With Time Delay Estimation

Time delay control is a control approach that estimates and compensates system uncertainties, including unmodeled dynamics and disturbances, through time-delayed signals of system variables. Thanks to its effectiveness and efficiency, TDC displays robust performance, although its compact structure is functional for systems with unknown or changing dynamics.

When matched with SMC, the combined approach, known as Sliding Mode Time Delay Estimation Control, enhances the system's robustness and reduces the chattering effects. SMTDEC utilizes Time Delay Estimation to approximate the effect of unmeasured dynamics and disturbances, so it can incorporate them into the control law, leading to improved system stability and performance.

The assumptions, to design a SMC with time delay estimation, are:

- system must be controllable and observable,
- unmeasurable dynamics and unexpected disturbances should be continuously differentiable,
- the TDE error must remain bounded.

By introducing sliding mode observers and disturbance observers, by the assumption of boundness and of immutability between two consecutive sampling moments, it is possible to provide an effective solution for systems subject to nonlinearities and uncertainties.

4.5 SMC of Induction Motor

Induction Motors are a mainstay in industrial applications due to their reliability and efficiency, despite their nonlinear dynamics and sensitivity to parameter variations. Sliding Mode Control offers a practical solution, providing robustness and disturbance rejection with minimum implementation complexity.

In the field-oriented control framework, SMC simplifies the decoupling and linearization of motor dynamics ($q - d$ coordinates); by transforming state and control variables into the stator flux-oriented reference frame ($\alpha - \beta$ coordinates), SMC facilitates the independent control of torque and flux, resulting in better performance and stability.

The integration of TDE into SMC for induction motors further improves system robustness by estimating and compensating for unknown rotor currents and external disturbances. In this context, the sliding surface is defined as the error between the desired and actual stator currents.

In conclusion Sliding Mode Control, as applied to discrete systems, offers robust and reliable performance, making it highly suitable for real-time digital applications. The addition of Time Delay Estimation enhances its effectiveness by addressing disturbances and uncertainties. When applied to induction motors, this combination achieves precise and robust control, meeting the demands of industrial applications.

5 Sliding Mode Control Design

The implementation of the Sliding Mode Controller (SMC) for the induction motor is based on dividing the control system into outer and inner loops. The outer loop is responsible for regulating the rotor speed to ensure it tracks the reference value, while the inner loop controls the current, which directly influences the motor's torque production.

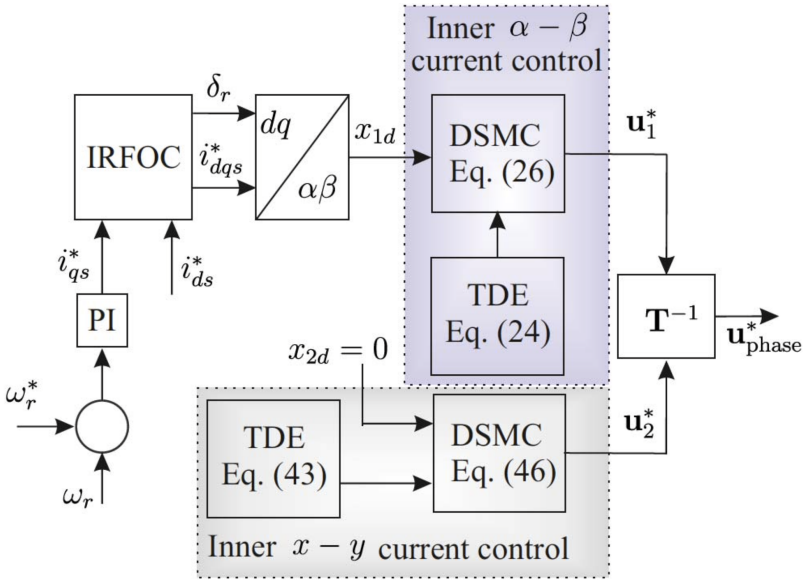

Figure 8: Block diagram of the proposed speed control based on IRFOC technique and the DSMC with TDE method for the inner current control.

5.1 Outer Control

The main goal of the outer control loop is to regulate the speed of the six-phase induction motor. To achieve this, a PI controller with saturation is used due to its simplicity and effectiveness in ensuring stable system dynamics. The PI controller is responsible for generating the dynamic reference current, i^*_{qs}, which is computed based on the deviation between the desired motor speed, ω^*_r, and the actual motor speed, ω_r.

An essential step in the outer loop is the estimation of the **slip frequency** ω_{sl}. This is carried out similarly to traditional indirect Rotor Field-Oriented Control (IRFOC) methods, relying on the reference currents i^*_{ds} and i^*_{qs} in the dynamic reference frame, as well as the electrical parameters of the six-phase induction motor.

The rotor angular position, $\delta_r(k)$, is calculated using the slip frequency, $\omega_{sl}(k)$, and the rotor speed, $\omega_r(k)$. The slip frequency is determined by the ratio of the reference currents, i^*_{qs} and i^*_{ds}, divided by the rotor time constant, $\tau_r = \frac{L_r}{R_r}$. This relationship is expressed as:

$$\omega_{sl}(k) = \frac{i_{qs}^*(k)}{i_{ds}^*(k)} \cdot \frac{1}{\tau_r} \tag{18}$$

The total rotor angular velocity, $\omega_{\text{tot}}(k)$, is the sum of the slip frequency and the rotor speed. The rotor angular position is updated recursively using the sampling period T_s with the following equation:

$$\delta_r(k+1) = (\omega_{sl}(k) + \omega_r(k))T_s + \delta_r(k) \tag{19}$$

The current reference generated by the outer loop serves as the input for the inner control loop. The inner loop employs a discrete sliding mode control (DSMC) with time-delay estimation (TDE) to ensure that the stator currents track the desired references accurately, even in the presence of uncertainties and unmeasured rotor currents.

The outer loop control system was implemented in Simulink. This loop ensures that the motor operates at the desired speed despite external disturbances or parameter variations.

The outer control loop consists of a PI speed controller which regulates the error signal produced by comparing electrical measured ω_r and reference speeds ω_r^*. It then produces the i_{qs}^* that together with the given i_{ds}^* allows to compute the δ_r. δ_r is then used in the Inverse Park Transform block which converts the desired quadrature and orthogonal currents (i_{qs}^*, i_{ds}^*) from the rotating $d-q$ frame to the stationary one $\alpha-\beta$. This block uses the following transformation:

$$\begin{bmatrix} i_\alpha \\ i_\beta \end{bmatrix} = \begin{bmatrix} \cos(\delta_r) & \sin(\delta_r) \\ -\sin(\delta_r) & \cos(\delta_r) \end{bmatrix} \begin{bmatrix} i_{ds}^* \\ i_{qs}^* \end{bmatrix} \tag{20}$$

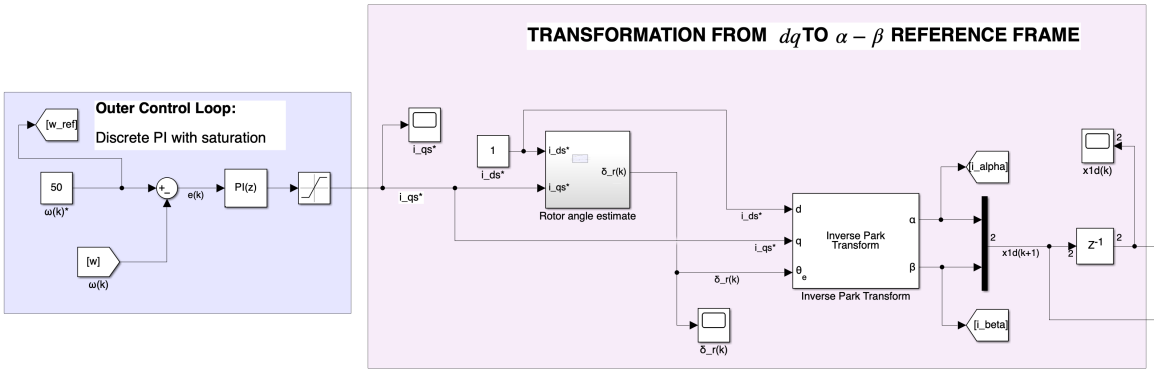

Figure 9: Simulink implementation of the outer loop control. The block computes the control signal $u(k)$ based on reference tracking and sliding mode control principles.

5.2 Inner Control

The aim of the inner loop is to control the stator currents. To that end, the DSMC with TDE method will be designed to force the stator current in the $\alpha - \beta$ and the $x-y$ subspaces to converge to their desired references in finite-time with high accuracy even in presence of unmeasurable states (i,e. rotor currents) and uncertainties.

5.2.1 Control of Stator Currents in the $\alpha - \beta$ Subspace

To define the control objective, let $x_1^d(k) = i_{s\phi}^*(k) \in \mathbb{R}^2$ represent the desired reference currents, with $\phi \in \{\alpha, \beta\}$. The tracking error is defined as:

$$e_\phi(k) = x_1(k) - x_1^d(k) = i_{s\phi}(k) - i_{s\phi}^*(k).$$

The sliding surface is selected as:

$$\sigma(k) = e_\phi(k).$$

For ideal sliding motion, the following conditions must be satisfied:

$$\sigma(k) = 0, \quad \sigma(k+1) = 0.$$

By substituting the system dynamics, $\sigma(k+1)$ is expressed as:

$$\sigma(k+1) = e_\phi(k+1) = x_1(k+1) - x_1^d(k+1),$$

$$\sigma(k+1) = A_1 x_1(k) + H_1 x_3(k) + B_1 u_1(k) + n_1(k) - x_1^d(k+1),$$

where $x_3(k)$ represents rotor currents and $n_1(k)$ denotes uncertainties.

To ensure robustness, a reaching law is adopted:

$$\sigma(k+1) = \lambda\sigma(k) - T_s\rho\text{sign}(\sigma(k)),$$

where $\lambda = \text{diag}(\lambda_1, \lambda_2)$ with $0 < \lambda_i < 1$, and $\rho \in \mathbb{R}^{2\times 2}$ is a positive diagonal matrix. The sign function $\text{sign}(\sigma_i(k)) = [\text{sign}(\sigma_1(k)), \text{sign}(\sigma_2(k))]^T$ is defined as:

$$\text{sign}(\sigma_i(k)) = \begin{cases} 1, & \text{if } \sigma_i(k) > 0, \\ 0, & \text{if } \sigma_i(k) = 0, \\ -1, & \text{if } \sigma_i(k) < 0. \end{cases}$$

Hence the discrete sliding mode control (DSMC) law for the stator currents in the α-β subspace is:

$$u_1(k) = -B_1^{-1}\left[A_1 x_1(k) - x_1^d(k+1) + \lambda\sigma(k) + H_1 x_3(k) + n_1(k) + T_s\rho\text{sign}(\sigma(k))\right].$$

Since the rotor currents $x_3(k)$ and uncertainties $n_1(k)$ are not measurable, the Time Delay Estimation (TDE) method is used. Assuming $x_3(k)$ and $n_1(k)$ do not vary significantly between consecutive samples, they are estimated as:

$$H_1\hat{x}_3(k) + \hat{n}_1(k) \approx H_1 x_3(k-1) + n_1(k-1),$$

$$H_1\hat{x}_3(k) + \hat{n}_1(k) = x_1(k) - A_1 x_1(k-1) - B_1 u_1(k-1).$$

The final DSMC with TDE control law is:

$$u_1(k) = B_1^{-1}\left[x_1^d(k+1) - A_1 x_1(k) - H_1\hat{x}_3(k) - \hat{n}_1(k) + \lambda\sigma(k) - T_s\rho\text{sign}(\sigma(k))\right]. \tag{21}$$

The Simulink blocks used for the implementation in the $\alpha - \beta$ subspace are the following:

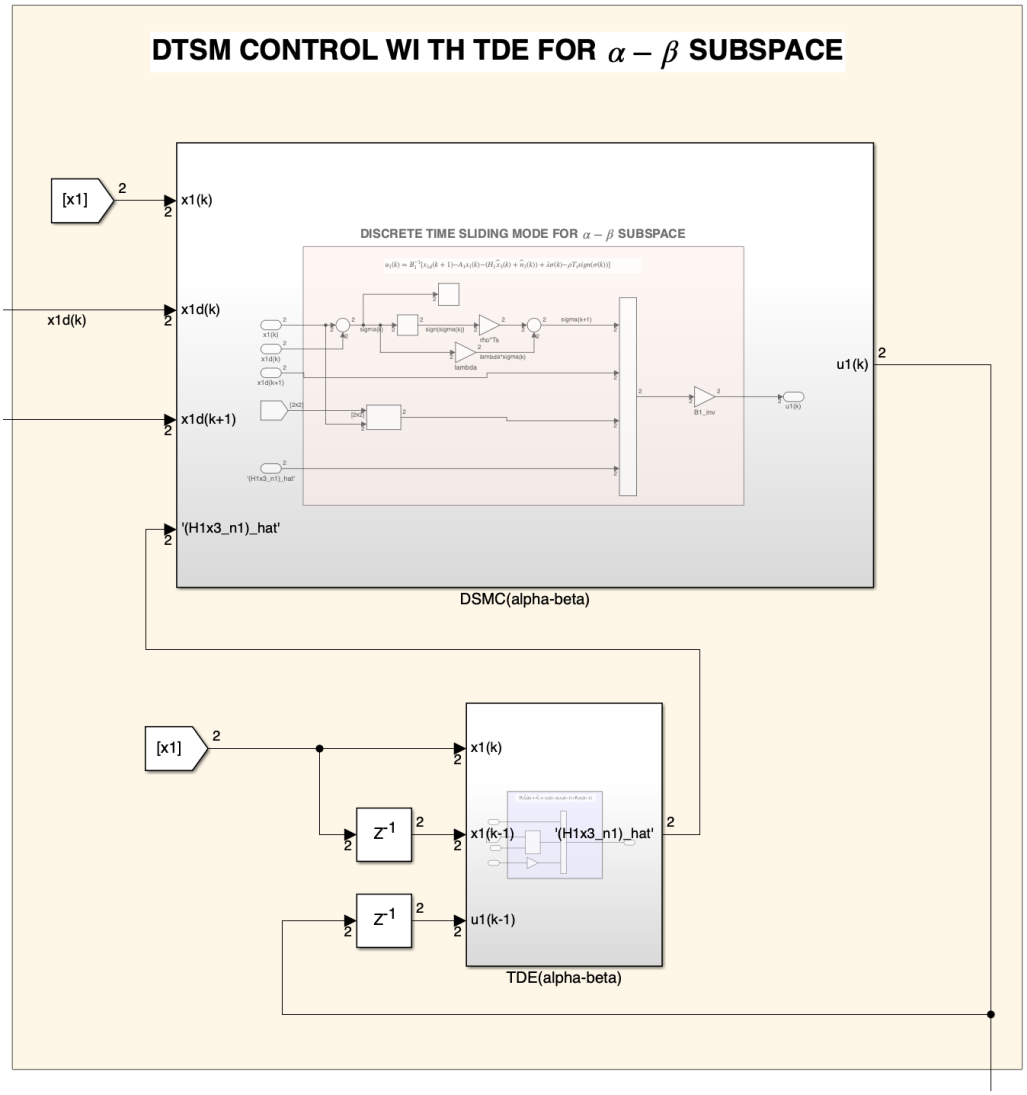

Figure 10: Simulink implementation of the inner loop control in the $\alpha - \beta$ subspace. It consists of a DSMC and a TDE.

where the DSMC computes the $u_1(k)$ as described by 21. The TDE block computes instead the term $H_1\hat{x}_3(k) + \hat{n}_1(k)$.

5.2.2 Control of Stator Currents in the $x - y$ Subspace

A similar methodology is applied for currents in the x-y subspace. The sliding surface is defined as:

$$\sigma^*(k) = e_{s_{xy}}(k) = x_2(k) - x_2^d(k),$$

where $x_2^d(k) = [i_{sx}^*(k), i_{sy}^*(k)]^\top$ are the desired reference currents. The discrete control law is:

$$u_2(k) = B_2^{-1}\left[x_2^d(k+1) - A_2x_2(k) - \hat{n}_2(k) + \Gamma\sigma^*(k) - T_s\varrho\text{sign}(\sigma^*(k))\right],$$

where $\hat{n}_2(k)$ is estimated using TDE:

$$\hat{n}_2(k) \approx x_2(k) - A_2x_2(k-1) - B_2u_2(k-1).$$

The sliding mode conditions are satisfied if the following inequalities hold for $i = 1, 2$:

$$\rho_i > \frac{\delta_i}{T_s}, \quad \varrho_i > \frac{\delta_i^*}{T_s}$$

where δ_i and δ_i^* are the upper bounds of TDE estimation errors.
Under these conditions, a quasi-sliding mode exists, ensuring finite-time convergence and robustness to uncertainties. The Simulink implementation for the $x - y$ subspace combines a Discrete-Time Sliding Mode Controller (DSMC) and a Time Delay Estimation (TDE) block. The DSMC block computes the control signal $\mathbf{u}_2(k)$ based on the sliding mode control law, using the desired state $\mathbf{x}_2^d(k)$ and the estimated disturbance $\hat{n}_2(k)$ from the TDE. The TDE block approximates disturbances by leveraging past state $\mathbf{x}_2(k-1)$ and control input $\mathbf{u}_2(k-1)$.

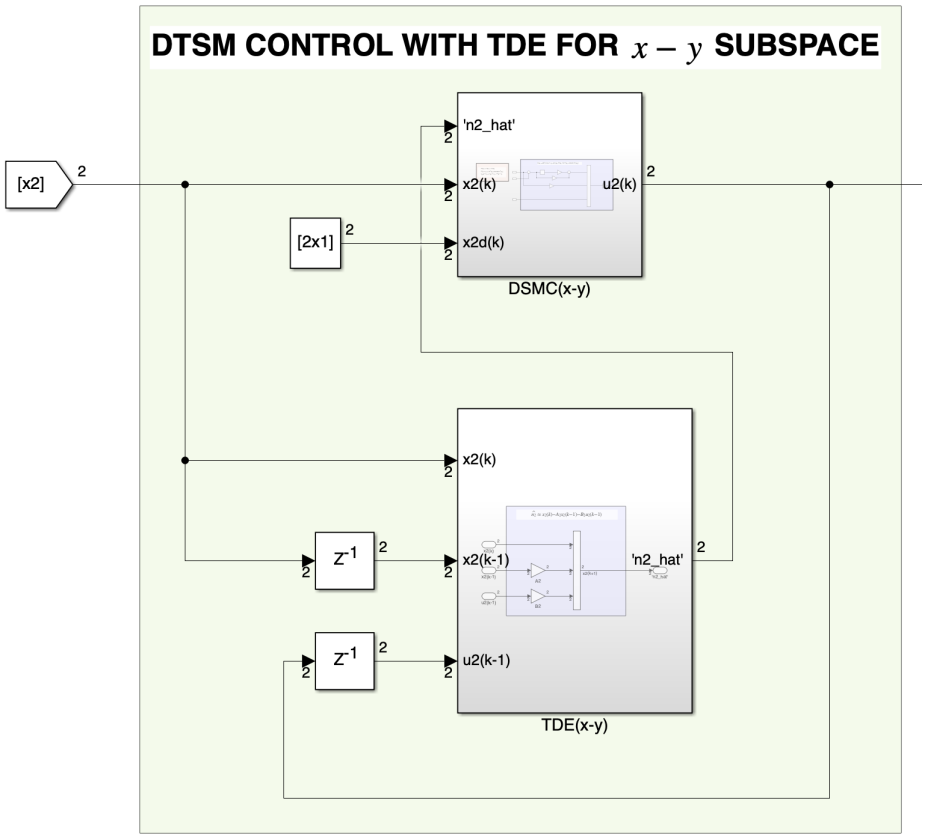

Figure 11: Simulink implementation of the inner loop control in the $x-y$ subspace. It consists of a DSMC and a TDE.

6 Simulation Results

The simulations were performed to evaluate the effectiveness of the proposed discrete controller, which combines Discrete Sliding Mode Control (DSMC) with Time Delay Estimation (TDE), applied to a six-phase induction motor. The main objectives were to assess the system's ability to accurately track the reference speed, regulate the stator currents in the $\alpha - \beta$ subspace, and ensure robustness against uncertainties and disturbances.

The motor model was implemented in Simulink with a sampling frequency of 10 kHz. The reference current for the d-axis was set to $i_{ds}^{*} = 1\,\text{A}$, while a load torque of 2 Nm was applied. The electrical and mechanical parameters of the motor, as well as the controller gains, were configured as detailed in the literature. Specifically, the PI controller gains were set to $K_p = 9.17$ and $K_I = 0.027$, while the DSMC gains in the $\alpha - \beta$ subspace were $\lambda = 0.5$ and $\rho_1 = \rho_2 = 30$.

The simulation results demonstrate the high performance of the proposed control strategy. Regarding speed tracking, the system achieved a Mean Squared Error (MSE) of 1.1457 rpm for a reference speed of 1500 rpm, confirming precise tracking performance during both transient and steady-state conditions.

In the $\alpha - \beta$ subspace, the average current tracking errors were 0.0575 A for the 1500 rpm reference speed. The tracking performance is illustrated in Figure 12 and Figure 13, with separate graphs showing the current tracking for the α and β components. These graphs indicate that the currents in both α and β converge smoothly to their respective references, demonstrating the controller's ability to effectively regulate the stator currents with minimal error.

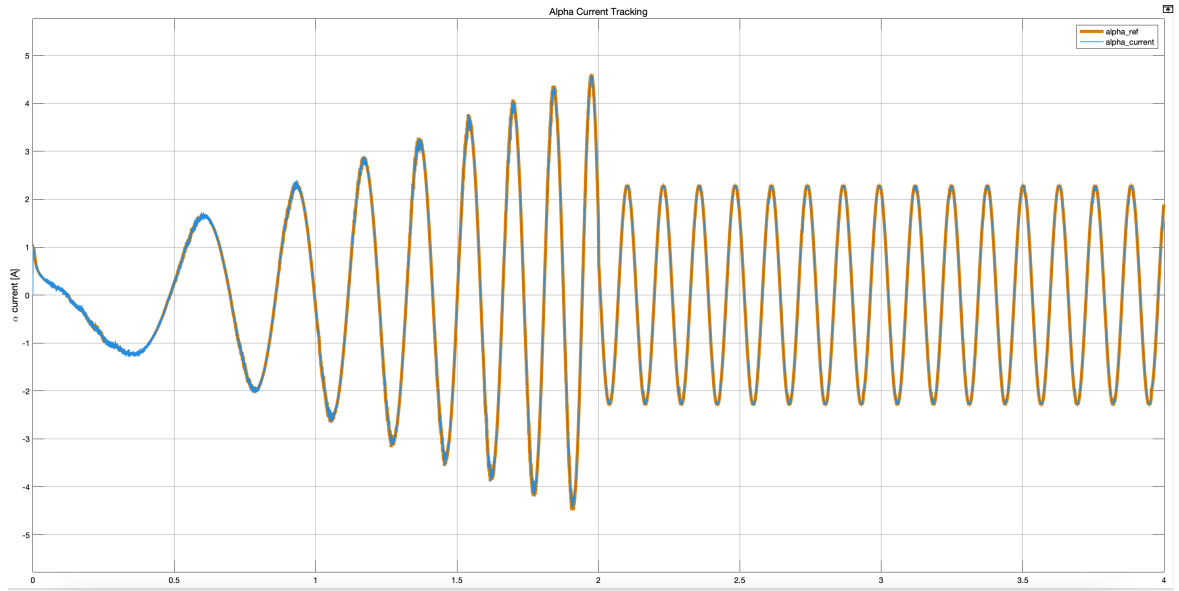

Figure 12: Current tracking in the α subspace for the reference speed of 1500 rpm.

Figures 14 and 15 show additional performance metrics. Figure 14 illustrates

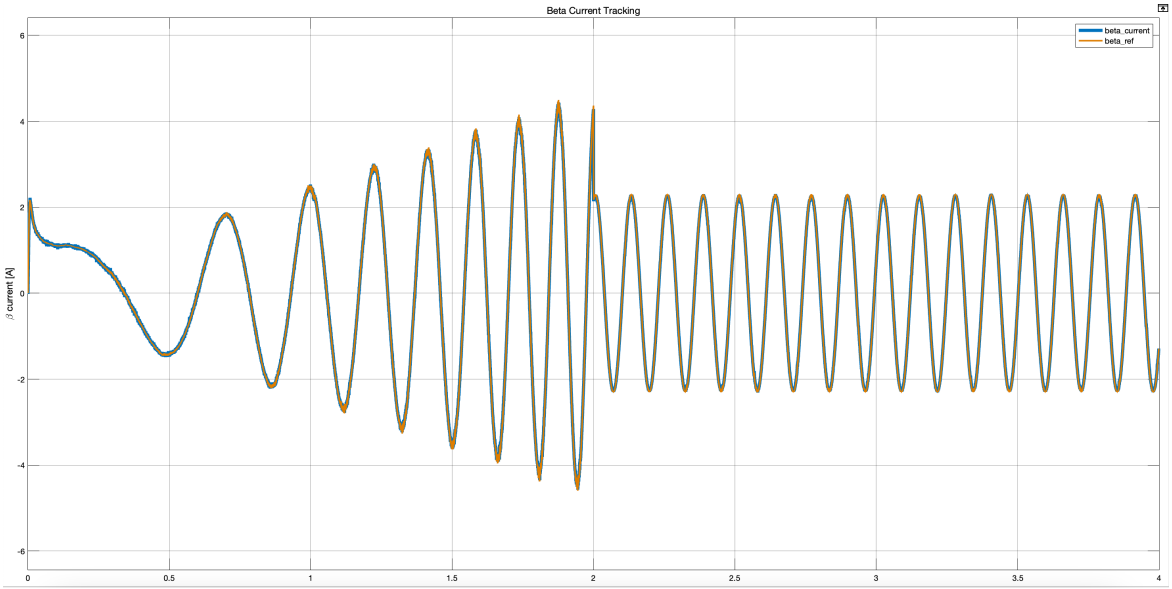

Figure 13: Current tracking in the β subspace for the reference speed of 1500 rpm.

the motor's ability to track the reference speed with minimal error, confirming the controller's robustness. Figure 15 shows the voltage signals generated by the control system and applied to the inverter to drive the motor.

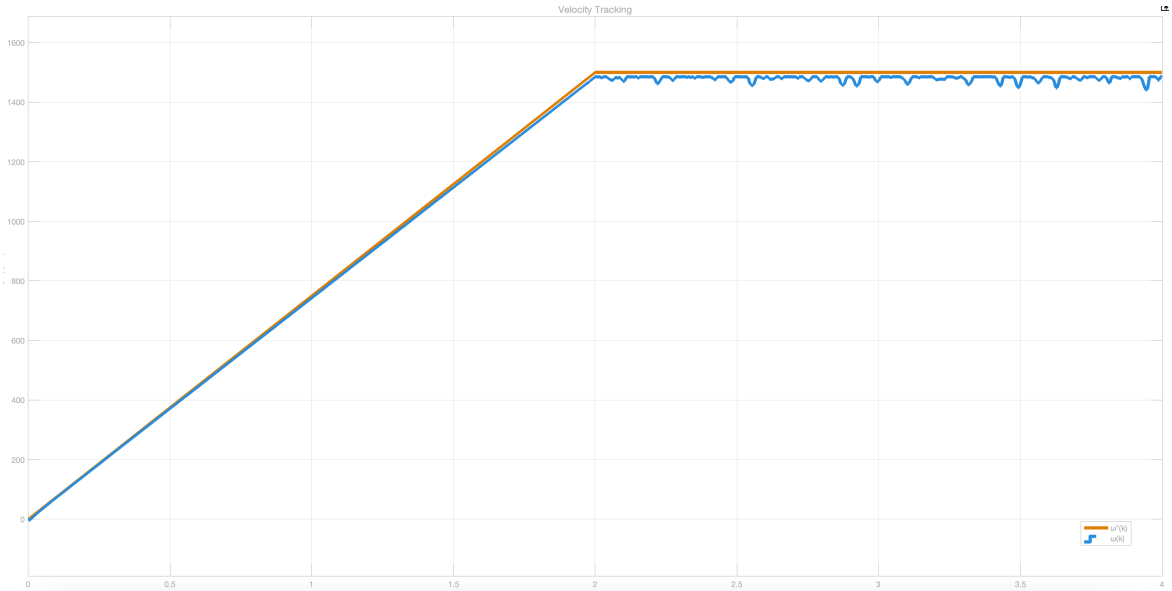

Figure 14: Motor speed tracking for reference speeds of 1500 rpm.

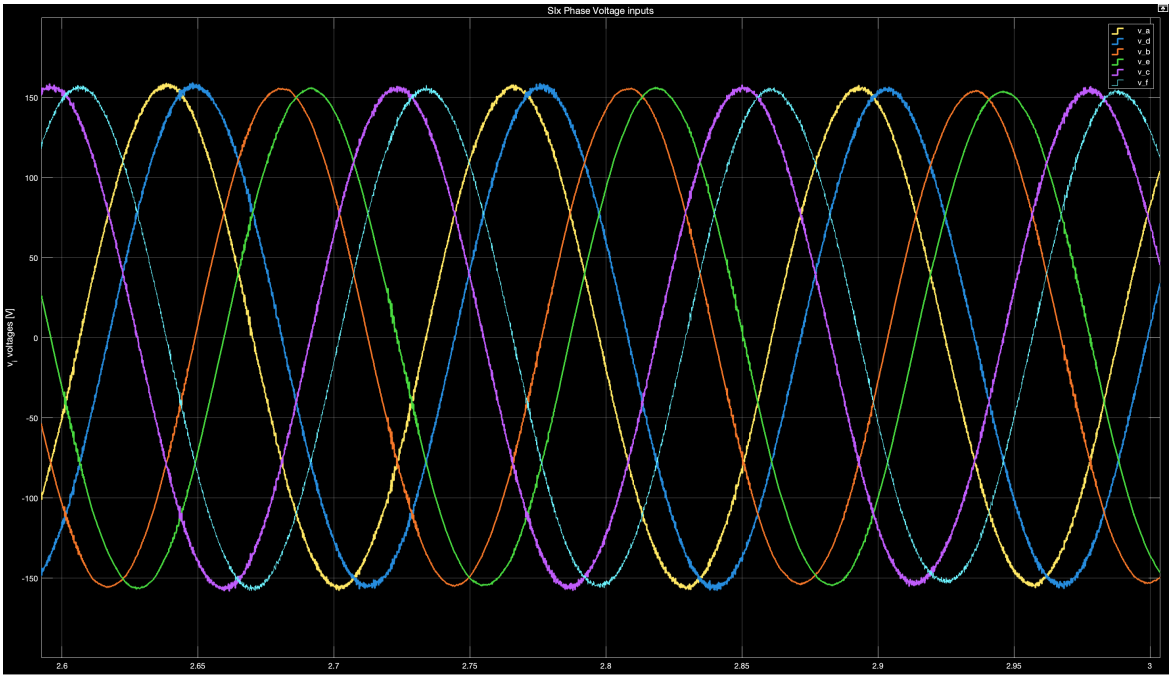

Figure 15: Voltage inputs generated by the control system and applied to the inverter.

In conclusion, the simulation results validate the robustness and precision of the proposed control strategy. The DSMC with TDE ensures rapid convergence of stator currents to their references, reduces chattering, and maintains excellent speed and current tracking performance.

7 Conclusions

There are many advantages in using this kind of control. In fact it is based TDE method that estimates Uncertainties and disturbances and on DSM that provides robustness Against TDE error, finite-time convergence and chattering reduction. The average switching frequency of the proposed method is lower than The conventional SMC and other controllers.

References

[1] Yassine Kali, Jorge Rodas, Magno Ayala, Maarouf Saad, Raúl Gregor, Khalid Benjelloun, Jesús Doval-Gandoy, and G Goodwin. Discrete-time sliding mode with time delay estimation of a six-phase induction motor drive. In *IECON 2018-44th Annual Conference of the IEEE Industrial Electronics Society*, pages 5807–5812. IEEE, 2018.

[2] Magno Ayala, Osvaldo Gonzalez, Jorge Rodas, Raul Gregor, Yassine Kali, and Pat Wheeler. Comparative study of non-linear controllers applied to a six-phase induction machine. In *2018 IEEE International Conference on Electrical Systems for Aircraft, Railway, Ship Propulsion and Road Vehicles & International Transportation Electrification Conference (ESARS-ITEC)*, pages 1–6. IEEE, 2018.

[3] Federico Barrero and Mario J. Duran. Recent advances in the design, modeling, and control of multiphase machines—part i. *IEEE Transactions on Industrial Electronics*, 63(1):449–458, 2016.

[4] Yassine Kali, Maarouf Saad, Khalid Benjelloun, and Mohammed Benbrahim. Sliding mode with time delay control for mimo nonlinear systems with unknown dynamics. In *2015 International Workshop on Recent Advances in Sliding Modes (RASM)*, pages 1–6, 2015.

[5] V. Bandal, B. Bandyopadhyay, and A.M. Kulkarni. Design of power system stabilizer using power rate reaching law based sliding mode control technique. In *2005 International Power Engineering Conference*, pages 923–928 Vol. 2, 2005.

[6] Je Hyung Jung, Pyung-Hun Chang, and Sang Hoon Kang. Stability analysis of discrete time delay control for nonlinear systems. In *2007 American Control Conference*, pages 5995–6002, 2007.